Comparing two passive location methods in a real environment

***Abstract*—**

***Index Terms*—Indoor localization, RSS, Passive localization, Comparison**

I. Introduction

XXXX

II. Problem Definition and Scenarios

Due to the availability of low energy-cost wireless sensors, we are witnesses of the wide and rapid diffusion of Wireless Sensor Network (WSN). The WSNs have been used in many promising applications such as health surveillance, battle field surveillance, and environmental monitoring. Localization is one of the most important subjects because the location information is typically useful for coverage, deployment, routing, location service, target tracking, and rescue.

The hardware infrastructures that can be used for the localization methods involve technologies based on acoustic signals, infrared signals and radio signals. All these infrastructures involve a set of devices or nodes known as Sensor Network (SN), which are deployed around the localization area, as figure 1 shows, where the nodes are black rounds. The localization methods can be used to localize the position of the sensor nodes or the position of the target, usually people or automotive devices. In the first case the positions of nodes must be estimated, while in the second case the position of nodes are known. The estimation of the node position within the network is named *node self-localization*. If the sensors are endowed with radio interfaces, the sensor network is named Wireless Sensor Network (WSN).

In general, in the localization application based on the SNs, the primary objective is to determine the location of the target measuring certain phenomena. The number of targets within the localization area can be one or more than one. In the first case, we refers to *single-target localization*, and in the second case we refer to *multiple-target localization*. If the sensor network is a WSN, the phenomena taken into account are the propagation of the radio signals and the multi-path due to the mesh of the Line of Sight (LoS) rays, among all the nodes of the WNS. Hence, another classification of the localization methods can be based on the phenomenon measured, such as the Received Signal Strength (RSS), the Time of Arrival (ToA), the Time Difference of Arrival (TDoA) and the Angle of Arrival (AoA) [1]. Briefly, the methods based on the measure of the RSS localize the target exploiting the relation between the power signal strength and the distance, or exploiting the relation between the multi-path interference (shadowing) and the target position. The methods based on the ToA and the TDoA take into account the relations between the propagation delay of the radio signals and the triangularization methods. Finally, the methods based on the AoA are based on the relations between the phase of the transmitted signal and the phase of the received signal at the antenna or at the array of antennas. Note that the kind of phenomenon measured depends on the technology adopted for the wireless sensors, i.e. sensors endowed with 802.11, as well as Ultra Wide Band (UWB) transceivers can measure the RSS and the ToA [2], [3], sensors endowed with multi-array antennas can also measure the AoA [1], sensors endowed with 802.15.4 transceiver can only measure the RSS [4]. Another way to classify the localization methods is based on the target characteristics. In fact, the target can transmit a radio signal or it can be a passive target. In the first two cases, we have active localization, in the last case we have passive or device-free localization.

The localization methods can also be classified through the localization scenario. In this case, the localization method can be classified in indoor and outdoor methods. Note that some methods adopted for the indoor localization can be used for the outdoor localization but not vice versa; for example WSNs can be used for indoor and outdoor localization but the outdoor methods based on the Global Positioning, which involves satellites, can not be adopted for indoor applications. Again, there may be no direct path among all the nodes of the WSN, because, specially in the indoor applications some obstacles can arise along the LoS between pairs of sensors. In this case we have the Non-LoS (NLoS) scenarios [5]. For the NLoS scenarios, the noise due to the reflection and diffraction increases so different models for the multi-path, as well as different localization techniques, must be adopted. Under these assumptions the localization algorithms can be classified for LoS and NLoS applications.

In this paper we argue about the localization and tracking algorithms for passive indoor applications, based on WSNs. The data used during the target's localization are captured by wireless sensors deployed in the surrounding of the localization area, and in LoS. In particular, our attention is toward the algorithms based on the measure of the Received Signal Strength (RSS), given that most of the existing wireless devices can provide this information. The RSS is a unit-less quantity used to measure the power of the received radio signal. Note that the RSS value is affected by many errors due to the battery charge and the antenna orientation, for example, so during the processing phase these aspects have to be taken into account. The data are collected through the N nodes named anchors. In general, the data collected from each sensor pair (a_i, a_j) named link, are formatted as a string with the following fields: the id of the receiver, the value of the sink, the RSS value measured between the receiver and others sensors, finally, the instant time at which the string was

acquired. Note that, in the literature taken into account for this paper all the authors assume that the links are not reciprocals $(a_i, a_j) \neq (a_j, a_i)$. Usually, the data are sequentially acquired, following the anchors numeration based on their ID, then the sampling rate is directly related to the number of used sensors. All the measured RSS values are sent to a laptop or a workstation by a base station named sink, which again is a wireless sensor node. Moreover, the sink broadcasts a ping in broadcast so that the anchors can reply sequentially with a message containing the node identification and the estimated transmitted power level.

The WSN used in this work for studying the performance of some algorithms, is based on the **IRIS Motes** wireless sensor nodes, produced by Crossbow [6]. This hardware is based on the high performance RF transceiver, **AT86RF230**, operating at 2.4GHz compliant with the IEEE 802.15.4 and ZigBee standards. The hardware can be programmed through a tool based on the **TinyOS** open source operating system, specifically designed for low-power wireless devices. The AT86RF230 can return the RSS value through two registers named **RSS_Val** and **ED** register, respectively. The first one is a 5-bits bit register, the second one is a 8-bit register, which holds the average value of the RSSs measured. The developed code to collect the data from the IRIS motes is based on the set of features already developed in a sample library known as **Spin Queues** .

The RSS values were collected during the movements of the human target (from now on named simply target) along a given path. The path is a sequence of steps equally distributed in the space. The target moves at a constant rate, with the aid of a metronome, in all the considered scenarios. In some scenarios the target walks, while in others the target runs. The RSS values show abruptly changes in time, even if the target is in a stable position. These changes are due to the multi-path and shadowing phenomena. So to capture the stochastic effect of these phenomena more experiments were carried out to better characterize the variables involved into the localization phase. The measurements were performed on different scenarios, with different number of sensors per squared meter of area, and different dimensions. Precisely, the number of sensors varies between 25 and 33, and the localization area varies between 28.8 m^2 and 54.6 m^2. For a given scenario, we captured a number of RSS's samples per link between 5 and 8. The localization area of each scenario was marked to create a lattice, as in the figure 1. Through this lattice the position of the target in the time has been evaluated and comparing esteemed position with the target's position in the lattice the localization error has been evaluated.

Some measures of the RSS have been performed using a multi-channel, on n_{ch} channels, or a single channel scanning. In general the number of RSS values of the links, available for the localization phase, are calculated as $N\,(N-1)n_{ch}$.

III. Algorithms Analysis

In general, the passive localization algorithms based on the RSS can rely on two main approaches for the target localization. The first is based on the estimation of some features linked to the target position through the measures of RSS [5], [7]–[9], and the second one is about the evaluation of the interfering image due to the target presence, named Radio Tomographic Approach [10].

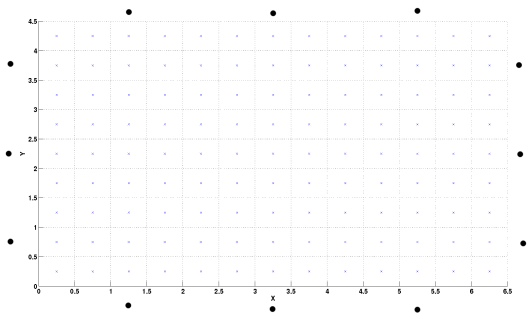

Fig. 1. Grid of the Localization Area

In the following the algorithms which adopt the methods introduced above are described. We provide an analysis of the algorithms through the study of the works based ob the passive localization, and then we show the performance of two of the algorithms taken into account in this paper, belonging to the two methods of prediction and Radio Tomography, respectively. In this way the theoretical as well as implementative aspects of the problem have been analyzed.

A. Prediction Method

1) : In [7], authors propose a method to estimate the probability $p(\mathbf{s}_t|\mathbf{x}_t)$ that the target position at the time t is $\mathbf{x}_t$, given the set of measures $\mathbf{s}_t$ by the Bayesian approach. This probability by the Bayesin Filter Theory [11] can be calculated as:

$$p(\mathbf{x}_t|\mathbf{s}_t) = \frac{p(\mathbf{s}_t|\mathbf{x}_t)p(\mathbf{x}_t|\mathbf{s}_{t-1})}{p(\mathbf{s}_t|\mathbf{s}_{t-1})} = p(\mathbf{s}_t|\mathbf{x}_t)\frac{\int p(\mathbf{x}_t|\mathbf{x}_{t-1})p(\mathbf{x}_{t-1}|\mathbf{s}_{t-1})d\mathbf{x}_{t-1}}{\int p(\mathbf{s}_t|\mathbf{x}_t)p(\mathbf{x}_t|\mathbf{s}_{t-1})d\mathbf{x}_t} \quad (1)$$

In the equation (1), the $p(\mathbf{s}_t|\mathbf{x}_t)$ is the probability density of measures conditioned by the target position. The integral at the numerator is the ChapmanKolmogorov equation used to evaluate the a-priori probability density function of the target's position. The a-priori information about the possible movements of the target is characterized by means of the probability density $p(\mathbf{x}_t|\mathbf{x}_{t-1})$, which describes the probability that the target is in the position $\mathbf{x}_t$, given that it was in the position $\mathbf{x}_{t-1}$. Finally, the denominator is the normalization value, which takes into account the space of all the possible evolutions of the measures given, the target's position. Finally, the position $\mathbf{x}_t$ belong to $\mathbb{R}^2$ where the components are the x and y coordinate in the space, and $\mathbf{s}_t$ belong to $\mathbb{R}^L$, where L is the number of links calculated as described in section II. The components of the vector $\mathbf{s}_t$ are the measures acquired link by link at time t.

The time variable t is discretized following the sampling interval used to acquire the values of RSS through the sensors.

Moreover, in this work the authors propose a model for the probability density of measures conditioned by the target position $p(\mathbf{x}_t|\mathbf{s}_t)$. For the model, authors assume that the measures are affected by Gaussian noise with mean $h(\mathbf{x_t})$ and variance $\sigma(\mathbf{x}_t)$, and that the measures per links are random variables identically and independently distributed (i.i.d). Then the conditioned distribution can be calculated as the product of the conditioned distribution per link

$$p(\mathbf{x}_t|\mathbf{s}_t) = \prod_L \frac{exp\{-\frac{(s_t^l - h^l(\mathbf{x}_t))^2}{2\sigma^l(\mathbf{x}_t)^2}\}}{\sqrt{2\pi\sigma^l(\mathbf{x}_t)}}$$

In this case s_t^l, $\sigma^l(\mathbf{x}_t)$ and $h^l(\mathbf{x}_t)$ are the measured values of RSS, the variance of the RSS and the average value of RSS for the link l, respectively.

The equation (1) can be solved through different methods such as the Grid-Based [12] and the Particle Swarm Filters [11]. Both methods solve numerically the equation, the main difference between two methods being the computational cost, which is largest for the Grid-Based approach. Given that the authors solve the equation with a Grid-Based approach, we analyze only this method. In this case, the localization area is represented by a grid with step Δ_x. The target's position $\mathbf{x}_t$ can be confined to the cells' grid, precisely the position of the target can be given by the center of the cells. Through this approach it is very simple to evaluate $h^l(\mathbf{x}_t)$ and $\sigma^l(\mathbf{x}_t)$. In fact, these values can be calculated cell per cell, acquiring the RSS values when the target place itself in the center of the cell. Note that smaller is the Δ_x smaller the error of the position estimation becomes, but the computational cost grows exponentially. Also the probability density $p(\mathbf{x}_t|\mathbf{x}_{t-1})$ can be defined by the grid. In fact, as the area's topology is known, we can define the probability that the target reaches the cell j, given that it is in cell i. For example, if the target can reach from the cell i n cells with the same probability, the probability to occupy one of them is $\frac{1}{n}$. A more rigorous study of this probability is proposed in [5], in this case the authors use the Hidden Markov Model to characterize the target's movements. Through the Grid-Based approach, the solution of the equation (1), which belongs to a continuos space, is approximated by the solution of the discretized space. By this approximation, the integrals can be relaxed in summation, obtaining the following recursive formulas:

$$p(\mathbf{x}_t|\mathbf{s}_t) = \sum_{j=cells} \omega_{t|t}^j \mathcal{I}(\mathbf{x}_t, \mathbf{x}_t^j); \quad (2)$$

$$p(\mathbf{x}_t|\mathbf{s}_{t-1}) = \sum_{j=cells} \omega_{t|t-1}^j \mathcal{I}(\mathbf{x}_t, \mathbf{x}_t^j); \quad (3)$$

$$\omega_{t|t-1}^j \triangleq \sum_{i=cells} \omega_{t-1|t-1}^i p(\mathbf{x}_t^j|\mathbf{x}_{t-1}^i); \quad j = 1 \dots cells; \quad (4)$$

$$\omega_{t|t}^j \triangleq \frac{\omega_{t|t-1}^j p(\mathbf{s}_t|\mathbf{x}_t^j)}{\sum_{i=cells} \omega_{t|t-1}^i p(\mathbf{s}_t|\mathbf{x}_t^i)}; \quad j = 1 \dots cells. \quad (5)$$

The values $\omega_{t|t}^j$ and $\omega_{t|t-1}^j$ in the equations (4, 5) are the weights used to approximate the integrals in the equation (1) through the Importance Sampling method into the discretize domain [13]. The function $\mathcal{I}(\mathbf{x}_t, \mathbf{x}_t^j)$ is the index function, which is 1 if the target position $\mathbf{x}_t$ coincides to the $j-th$ cell $\mathbf{x}_t^j$ and 0 otherwise.

Equations (2, 3, 4, 5) allow to evaluate the probability map of the target position in the time by using the acquired values of RSS.

2) : In [9], authors propose a localization algorithm based on the learning by example (LBE) strategy to localize and track passive target. The localization problem is addressed only by considering the available RSS values at the nodes of the wireless sensor network deployed in the localization environment.

The authors assume that in the localization area a WSN with N nodes (anchors) is deployed. The unknown target moves throughout the two-dimensional investigation domain. Each anchor a_j $j = 1 \dots N$ is a transceiver located in a known position (x_{a_j}, y_{a_j}) $j = 1 \dots N$. Under the assumption that each node communicates with all the remaining $N-1$ nodes, a total amount of $L = N(N-1)$ wireless links are available. The measured value of signal strength s_j^i on the link $l = (a_i, a_j)$ depends on the interactions among the electromagnetic signal radiated by the $i-th$ source, the localization scenario, and the targets to be localized.

To distinguish the impact of the target's mote on the RSS values from the impact of the surrounding environment, the calibration measure of the RSS values is performed when no target is present in the area $\hat{s}_j^i$. The contribution of the surrounding environment is filtered out from the RSS measures, when the target is in the area s_j^i, as in the following equation:

$$\Gamma_{ij} = \frac{s_j^i - \hat{s}_j^i}{\hat{s}_j^i}; \quad (6)$$
$$i = 1 \dots N; \; j = 1 \dots N-1.$$

We refer to equation (6) as the differential measure of the RSS values. The differential measure is acquired for all the WSN's links $\mathbf{\Gamma} = \{\Gamma_{ij};\ i = 1 \dots N;\ j = 1 \dots N-1\}$. Starting from the differential measurements $\mathbf{\Gamma}$, the addressed problem is about the definition of the probability that the target lies in a given position $\mathbf{x} = [x, y]$ of the localization area. To evaluate the probability the authors adopt the classification techniques based on Support Vector Machines (SVM).

The SVM method [14], [15] is a learning model with associated learning algorithms that analyze data and recognize patterns, used for classification and regression analysis. The basic SVM takes a set of input data and predicts, for each given input, which of two possible classes forms the output. Given a set of training examples, each marked as belonging to one of two categories, a SVM training algorithm builds a model that assigns new examples into one category or the other. A SVM model is a representation of the examples as points in space, mapped so that the examples of the separate categories are divided by a clear gap that is as wide as possible. New examples are then mapped into that same space and predicted to belong to a category based on which side of the gap they fall on.

The SVM methods need R training configurations Δ,

$$\Delta = \{(\Gamma, \mathbf{x}_m, v_m)_r \; r = 1 \dots R\} \tag{7}$$

given by the set of differential measurements $\mathbf{\Gamma}$, a random position $\mathbf{x}_m$ with associated the state

$$v_m = \begin{cases} 1 & \text{if the target is in } \mathbf{x}_m \\ -1 & \text{otherwise.} \end{cases}$$

During the so called training phase, the training set are used to find a suitable decision function Φ by means of a SVM strategy [14], [15]. Assuming that the localization area is a lattice with C squared cells as shown in the figure 1, the authors define the decision function for the given cell c, by the following equation:

$$\Phi(\mathbf{\Gamma}, v_c) = \sum_{p=1}^{C}\sum_{r=1}^{R}\left\{\alpha_c^r v_c^r \Theta(\mathbf{\Gamma}^{(r)}, \mathbf{\Gamma}^{(p)}, p, c)\right\} + \frac{\sum_{p=1}^{C}\sum_{r=1}^{R_{sv}}\left\{v_c^r - \sum_{p=1}^{C}\sum_{r=1}^{R}\left\{\alpha_c^r \Theta(\mathbf{\Gamma}^{(r)}, \mathbf{\Gamma}^{(p)}, p, c)\right\}\right\}}{R_{sv}} \tag{8}$$

where $\Theta(\cdot)$ is the kernel function adopted for the problem addressed, the α's values are the Lagrange multipliers of the optimization problem associated with the SVM problem addressed, and R_{sv} is the support vector, i.e. the set of training data where the Lagrangian multipliers for the cell c are not equal to zero. For more details in [16] an in-depth analysis of the problem is provided.

Through the decision function, the classification problem can be defined as a binary classification problem, using the sign function, which, for given value of the decision function, returns the binary states:

$$\mathbf{v} = sign[\Phi(\mathbf{\Gamma})]\mathbf{v} = \{v_c \; c = 1 : \dots C\}.$$

Note that the sign of the decision function can be replaced by the a-posteriori probability $Pr\{\mathbf{v} = 1|\mathbf{\Gamma}\}$ [17] to construct a location-probability map of the monitored area. The a-posteriori probability gives information about the degree of membership of test data to a particular class, even if $sign[\Phi(\mathbf{\Gamma})]$ does not correctly classify the input pattern. This behavior is mainly due to the generalization capabilities of the SVM approach that, in presence of highly non-separable data, constructs the best separating hyperplane even if the optimal solution to the optimization problem [15] does not exists. In this way, the input test data could belong to the wrong half-plane identified by the decision function. However, taking into consideration the a-posteriori probability it is still possible to compute the distance of that example to each class means.

The mapping between the state information and the a-posteriori probability can be provided by the following equation:

$$Pr\{v_c = 1|\mathbf{\Gamma}\} = \frac{1}{1 + exp\{\gamma\Phi(\mathbf{\Gamma}, v_c) + \delta\}} \tag{9}$$

where the parameters γ and δ can be calculated resolving the optimization problem of a cost function of the training data set, as shown in [16].

Finally the esteemed target position can be calculated as in the following:

$$\hat{x} = \frac{\sum_{c=1}^{C} xPr\{v_c = 1|\mathbf{\Gamma}\}}{\sum_{c=1}^{C} Pr\{v_c = 1|\mathbf{\Gamma}\}} \tag{10}$$

$$\hat{y} = \frac{\sum_{c=1}^{C} yPr\{v_c = 1|\mathbf{\Gamma}\}}{\sum_{c=1}^{C} Pr\{v_c = 1|\mathbf{\Gamma}\}} \tag{11}$$

3) : In [8], authors propose a localization algorithm that works in two phases: the short offline phase, during which the algorithm studies the features of the signal strength (RSS) values when no target is present inside, and the monitoring phase, where the target position is esteemed by detecting the anomalies in the features of the RSS values. The two phases of the algorithm are achieved by difference modules.

The first module of the algorithm is the Normal Profile Construction. In this module, the *features* of the RSS values are calculated. Typical features are the mean value, the dispersion or the variance. The authors, by several measurements assume as features the standard deviation or the variance, given that this feature has high sensitivity to the target motion, and it shows a good stability in time. Let's assume that in the sensor network there are a set of transmitting nodes, or Access Points (APs), and a set of receiving nodes, or Measuring Points (MPs). The MPs acquire the RSS values of the signals transmitted by the APs. The overall number of links, between any pair of AP-MP, is L, which is he number of APs times the number of MPs. The received signals strengths (RSSs) s_t^j for the link j at the time instant t, are acquired by a sliding window of length l, $W_t^j = [s_{t-l}^j s_{t-l+1}^j \dots s_t^j]$. The values in the window W_t^j are mapped in the feature of the RSS values f_t^j through a function $g(W_t^j)$. This module calculates the features assuming that no target is present in the area. Finally, the Normal Profile is obtained evaluating the density distribution of the features through a non-parametric estimation method [18]. This method fits, by a set of Kernel function, a given set of empirical data with the introduction of as little extraneous information as possible. In this case, the authors use as empirical data the features of the RSS values per link evaluated in n different windows, $f_1^j \cdots f_n^j, \; j = 1 \cdots L$, and as kernel functions the Epanechnikov's function. The density distribution for the features of the link j can then be calculated as:

$$\hat{u}_j(f) = \frac{1}{nh_j}\sum_{i=1}^{n} K\left(\frac{f - f_i^j}{h_j}\right); \quad (12)$$
$$K(y) = \begin{cases} \frac{3}{4}(1-y^2) & \text{if} |y| \leq 1 \\ 0 & \text{otherwise} \end{cases}$$
$$h_j = 2.345\sigma_j n^{-0.2}$$

where σ_j is the variance of the samples of the link j and h_j is the bandwidth of the distribution.

In the Basic Detection Module signal strength anomalies, due to the target presence, are detected. The detection is based on the normal profiles constructed during the offline phase. In particular, for a window of samples W_t^j for the link j at a given time instant t, the module calculates the corresponding feature value f_t^j i.e. the sample variance. Then the RSS values of the link j are considered anomalous if f_t^j is above a critical bound b_j . This bound is calculated as the α-th percentile of the Cumulative Distribution Function (CDF) $\hat{F}_j$ of the feature density distribution evaluated by the equation (12) as $b_j = \hat{F}^{-1}(1-\alpha)$. From the Basic Detection Module an alarm arises when any set of values per link is anomalous. This approach can lead to many false positives, so the final decision is improved through the Decision Refinement Module.

Due to the dynamic changes in the environment, the stored profiles may not capture the real normal state. Therefore, the systems needs to update the stored profiles during the online phase. Authors update the density distribution with the new samples f^j by the following weighted equation:

$$\hat{u}_j(f) = \frac{1}{nh_j}\sum_{i=1}^{n} w_i K\left(\frac{f - f_i^j}{h_j}\right) \quad (13)$$
$$w_i = \frac{i}{n(n+1)/2}.$$

By this formula the new data are more relevant than the old data for the estimation of the the normal profiles.

The Decision Refinement Module assigns to the RSS values of the link j at the time t, the anomaly score $A_t^j = \frac{f_t^j}{b_j}$. Then the module studies the behavior of a global anomaly score A_t, calculated as the summation of the singles values of the anomaly scores for each link. If a noticeable change in A_t occurs, while at least the values of one link are anomalous, then an anomalous behavior is starting. The module makes use of the history of the activity state inside the environment through the usage of exponential smoothing to monitor the a_t in order to avoid the noisy samples, hence reducing the false alarm rate. Moreover, the authors note that, during the target motion, the same or near links are affected by the motion. Hence, the sum of anomalies has higher values during the motion period.

Finally, the localization information is provided by the Region Tracking User Interface Module. The system provides the graphic map where the localization information is shown in terms of the most probable regions of the detected event. In this case, the information about the anomaly score for each set of RSS values per link is used, jointly with the distance of each pixel of the map from each link.

B. Radio Tomography Method

Was adopted the common assumption of 2-D localization since the third dimension usually in not of primary interest in an indoor environment.

In [10], authors study the application of the Radio Tomographic Imaging (RTI) to a wireless sensor network. Roughly speaking, this method provides the image of the attenuation in the RSS due to the target within the wireless network. Precisely, the authors localize the target by studying the Variance of the Radio Tomographic Image (VRTI).

The method can be stated as in the following. Let $\{a_1, \ldots, a_n\}$ be the anchor set, with known positions. The anchor pair (a_i, a_j) is a link l of the wireless network, the total number of links L is calculated as described within the section II. The network area is conventionally divided into P pixels, so the movement of the target is discretized on the pixel set.

The problem is to find a mapping that links the variance per link to the variance per pixel of the RSS's values. The authors in this work adopt a linear model

$$\mathbf{s} = W\mathbf{s}_{px} + \mathbf{n} \quad (14)$$

where $\mathbf{s}_{px} \in \mathbb{R}^P$ is the RTI over the pixel set, so s_{px_i} is the variances of the RSS value for the $i-th$ pixel, $\mathbf{s} \in \mathbb{R}^L$ is the vector of the measured values of variance over the set of links, $\mathbf{n} \in \mathbb{R}^L$ is the noise of the measures, and finally $W \in \mathbb{R}^{LxP}$ is the mapping matrix whose entries are the weights that link the pixels to the variance per link.

The weights of the mapping matrix W can be calculated assuming that the power of the received signal is proportional to the inverse of the squared distance covered by the signal, and that the target crossing a link (a_i, a_j) influences a set of pixels. Precisely, the authors assume that the set of influenced pixels fall within within the area limited by an ellipse. Hence, for the weights of the matrix W the following equation is applied:

$$w_{ij} = \frac{1}{\sqrt{LoS}} \begin{cases} \phi & \text{if } d_{ij}^1 + d_{ij}^2 < LoS + \lambda \\ 0 & \text{otherwise} \end{cases} \quad (15)$$

where LoS is the distance of the line of sight between two nodes , d_{ij}^1 and d_{ij}^2 are the distances from the center of pixel j to the two node locations for link i, and λ is a tunable parameter describing the width of the ellipse. The parameter λ is typically set very low usually in the range $[0.1-0.6]$ (m). The ellipsoid is primarily used to simplify the process of determining which pixels fall along the LoS path, as showed in the figure 2 by the green pixels. Finally, the parameter ϕ is a scaling factor to normalize the RTI, typical values are into the interval $1 - 100(dB)^2$.

The model estimation of the variance per pixel in the equation (14) provides a mathematical framework to relate the target's movement in space to a links RSS variance. The model is an ill-posed inverse problem that is highly sensitive to measurement and modeling noise. The solution $\mathbf{s}_{px}$ can be calculated by the least-squares approach, but the solution can not be unique, hence the regularization method [19] must be applied to obtain the solution. In this work, the authors propose as regularization method the Tikhonov's method. Through the

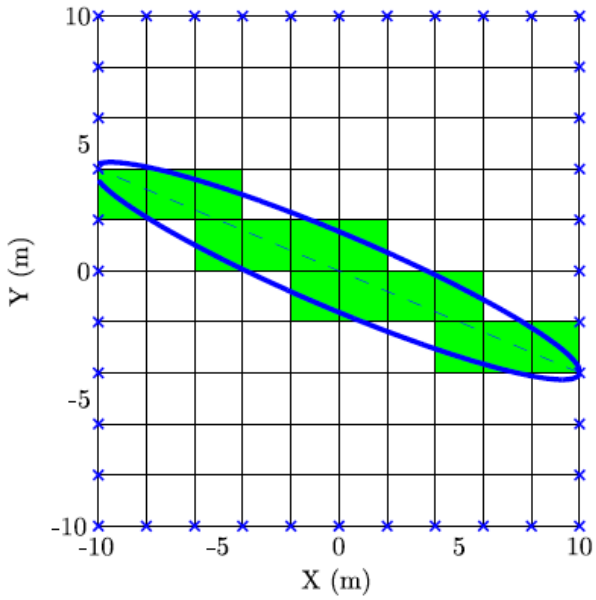

Fig. 2. Representation of pixels involved along the LoS path.

Tikhonov method the least-squares problem that needs to be revolved is:

$$\hat{\mathbf{s}}_{px} = arg\min_{\mathbf{s}_{px}} \frac{1}{2}||W\mathbf{s}_{px} - \mathbf{s}||^2 + \alpha||Q\mathbf{s}_{px}|| \qquad (16)$$

where $Q$is the Tikhonov's matrix that produces the solution with the desired properties, and α is a tunable regularization parameter. To calculate the parameter α many algorithms have been developed [20]. The least-squares problem's solution can be calculated by the following equation:

$$\hat{\mathbf{s}}_{px} = (W'W + \alpha Q'Q)^{-1}W'\mathbf{s}. \qquad (17)$$

As stated above, the matrix Q captures some features of the measured acquired. Taking into account the covariance matrix C as well as the variance σ_N^2 of the noise process linked to the measures, the solution in the equation (17) can be calculated as:

$$\hat{\mathbf{s}}_{px} = (W'W + \sigma_N^2 C^{-1})^{-1}W'\mathbf{s}. \qquad (18)$$

The entries c_{ij} of the covariance matrix C can be calculated assuming that the spatial attenuation of the field decays with exponential law [21]

$$c_{ij} = \sigma^2 exp\left(-\frac{d_{ij}}{\delta_c}\right) \qquad (19)$$

where d_{ij} is the distance between centers of pixels i and j, σ^2 is the variance of pixel attenuation, and δ_c is a correlation parameter that can be used to determine the desired amount of smoothness in the image. The target's coordinates $\mathbf{x} = [x\ y]$ are the coordinates of the maximum value in the vector $\hat{\mathbf{s}}_{px}$ calculated by the regularization method.

Finally the authors develop the tracking algorithm based on the VRTI values through the Kalman's filter as in the following:

$$\begin{aligned} \hat{V} &= V + \sigma_m^2 I_2; \\ G &= \hat{V}(\hat{V} + \sigma_n^2 I_2)^{-1} \\ \hat{\mathbf{x}} &= \hat{\mathbf{x}} + G(\mathbf{x} - \hat{\mathbf{x}}) \\ V &= (I_2 - G)\hat{V} \end{aligned} \qquad (20)$$

where I_2 is the 2×2 identity matrix, σ_m^2 is the variance of the targets motion process, indicating how fast the object is capable of moving. Larger values enable the filter to track faster moving objects. Authors also take into account σ_n^2 that is the variance of the measurement noise. Larger values will cause the filter to trust the statistical predictions over the instantaneous measurements. The vector $\hat{\mathbf{x}}$ contains the Kalman esteemed coordinates x and y. $\mathbf{x}$ is a two-element vector containing the instantaneous measurement of the target coordinates through the VRTI method. $\hat{V}$ is the a priori error covariance matrix and V is the a posteriori error covariance matrix and finally G the Kalman Gain. Note that authors provide some values for these parameters through a set of measurements performed during their experiments.

In this case the coordinates of the target position are the coordinates of the maximum of the vector $\hat{\mathbf{s}}_{px}$ or the coordinates $\hat{\mathbf{x}}$ filtered out by the Kalman altorithm.

IV. Numerical Results

The numerical results discussed in this section are obtained by both measurements performed with the WNS deployed by us, as discussed in the section II and by the repository of data making available by the SPAN laboratory at University of Utah on Internet. The performance of the algorithms described into the section III are analyzed for the following scenarios:

TABLE I
SCENARIOS

Scenario	Area(m^2)	Anchors	Channels	Speed (m/s)
1	6.4×4.5	25	1	0.25
2	6.5×4.5	28	1	0.915
3	6.5×4.5	28	1	1.83
4	6.5×8.4	33	5	0.45

where $Channel$ is the number of wireless channels used to acquire the RSS values, and $Speed$ is the target's peed along the path.

We have developed the localization algorithms, as well as the data elaboration modules by means of the MATLAB tool.

The performance parameters are related with the error $\epsilon = \sqrt{((x-\hat{x})^2 + (y-\hat{y})^2)}$, where x, y and $\hat{x}$, $\hat{y}$ are the components of the position and the estimated position of the target, respectively. Precisely, the parameters taken into account are the Mean Squared Error (MSE) of the estimated positions, and the $70-th$ and $90-th$ percentile of the estimation error. Moreover, figures about the estimation error distribution are shown in the following.

The performance discussed in the following are about the **Scenario 1**. First the results on the Bayesian method are presented, and later those one on the Tomographic approach.

The Bayesian method has been applied on the lattice with 9×13 cells, the area per cell was about $0.5 \times 0.5\, m^2$. The Calibration phase, discussed in section III-A1, has involved the estimation of the average and variance h^l and σ^l, respectively, of the RSS values per link without presence of target. The transition probability $p(\mathbf{x}_t|\mathbf{x}_{t-1})$ has been defined through a matrix $\mathcal{M}$ where the entry m_{ij} is the probability that the target from the cell i goes to the cell j. Finally, we assume that the initial probability $p(\mathbf{x}_0)$ is 1. This information is used for the resolution of the recursive problem in the equations (2, 3, 5, 4). We assume that the target moves with steps of one cell, hence the cells with distance one step from the target can be reached with equal probability, otherwise with probability zero. Figure (3) shows the distribution of the error of the estimated position, precisely, the figure 3(a) shows the error distribution assuming that the target can move toward any cell with distance 1, while the figure 3(b) shows the error distribution when some obstacles are considered along the path so that some cells with distance 1 become unreachable.

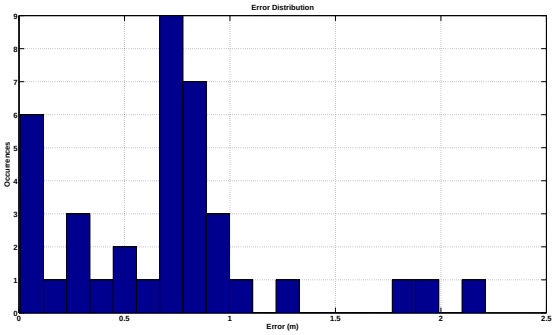

(a)

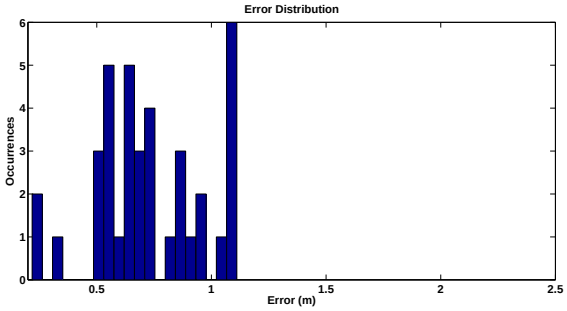

(b)

Fig. 3. Error Distribution Bayesian Method Scenario 1

The figures show that the knowledge of the target movement significantly affects the error estimation. In fact, the estimation error increases of the 12.6%, decreasing information on about 23% of the cells. Moreover, increasing the knowledge it is possible to bound the dispersion of the error values. Note that in the case with more information on the target movements the dispersion of the error values decreases of about 50% . The values in the Table II confirm these results. The values in the first row are relevant to the case with less knowledge on the target's movements.

The reason is that, in this last case, the number of indeterminate states reachable by the target grows. Instead, when we can limit the target's movement the stochastic process that underlies to it results like constrained.

TABLE II
PERFORMANCE PARAMETERS SCENARIO 1 BAYESIAN METHOD

RMSE (m)	75-th percentile (m)	90-th percentile (m)
0.87	0.88	1.23
0.77	0.9	1.1

The Tomographic method has been applied on the **Scenario 1** using the algorithm's parameters shown in tableIII. The method has been tested assuming the solution for the VRTI that in the equation (17) first and in the equation (18) later. In the first case the matrix Q is the identity matrix.

TABLE III
TOMOGRAPHIC ALGORITHM'S PARAMETERS

$\lambda\ (m)$	$\sigma\ (dB)$	σ_N	δ_c	σ_m	σ_n	$\Phi\ (dB)^2$
0.1	0.3	1	3	0.1	5	60

Moreover, the values of the estimated position have been filtered out through the Kalman's filter to study the improvement of the performance estimation.

Figure 4 shows the distribution of the localization error using the Tomographic method assuming the equation 18 as a solution of the VRTI.

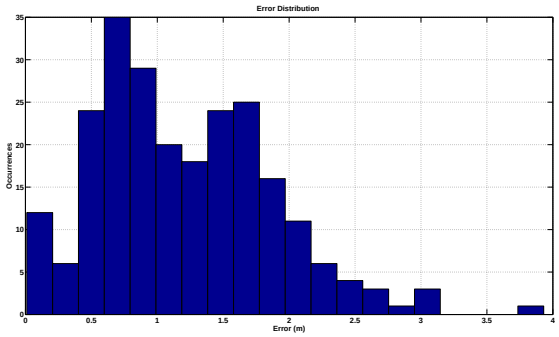

(a)

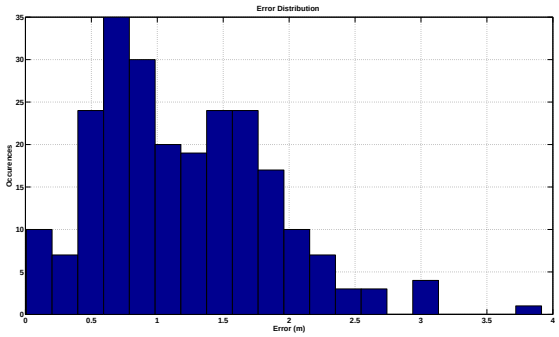

(b)

Fig. 4. Error Distribution Tomographic Method Scenario 1

The figure 4(a) shows the error distribution when only

the VRTI is used, instead the figure 4(b) shows the error distribution when the estimated position is also filtered out by Kalman. The figures show that the Kalman filter does not improve the method's performance. In fact, the dispersion of the error values is the same as well as the interval of errors with the maximum number of occurrences. These results are confirmed by the performance parameters shown in table IV.

TABLE IV
PERFORMANCE PARAMETERS SCENARIO 1 TOMOGRAPHIC METHOD

RMSE (m)	75-th percentile (m)	90-th percentile (m)
1.60	1.95	2.70
1.58	1.93	2.62

The values in the first row of the table **??** are relevant to the VRTI estimation only, while the values in the second row are about the VRTI values filtered out by the Kalman's filter. Even if the Kalman filter does not give advantage in the position estimation, note that through it also the speed of the target can be estimated if the target moves of constant velocity.

Figure (5) shows the distribution of the localization error using the Tomographic method, assuming equation 17 as a solution of the VRTI, which we call Un-Noised model.

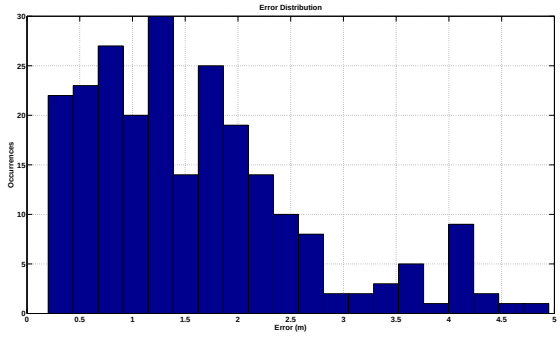

(a)

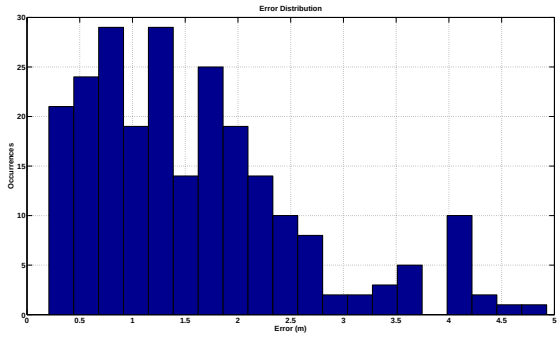

(b)

Fig. 5. Error Distribution Tomographic Method Un-Noised Scenario 1

Figure 5(a) shows the error distribution when only the VRTI is used, while the picture 5(b) shows the error distribution when the estimated position is also filtered out by Kalman. In this case too, the Kalman's filter does not give advantage, as shown in table V .

TABLE V
PERFORMANCE PARAMETERS SCENARIO 1 TOMOGRAPHIC METHOD UN-NOISED MODEL

RMSE (m)	75-th percentile (m)	90-th percentile (m)
2.55	3.28	3.78
2.54	3.28	3.77

The error reduction is notable when the equation 18 is used as a solution for the VRTI instead of equation 17. In this case, the localization error can be decreased about of 59%, moreover, the error dispersion is lower with the first solution than the second one, as the figures 4 and 5 show.

In the following, the figures about the performance of the Bayesian and Tomographic methods on the **Scenario 2** and **Scenario 3** are shown. The considerations made for the **Scenario 1** hold true, also for these two scenarios.

For **Scenario 2** and **Scenario 3**, the Bayesian method has been applied on the lattice with 10×14 cells, the area per cell was about $0.45 \times 0.45\, m^2$

Figure 6 shows the distribution of the localization error for the Bayesian method for the scenarios 2 and 3. Precisely, figure 6(a) shows the error distribution for the **Scenario 2** and the figure 6(b) for the **Scenario3**.

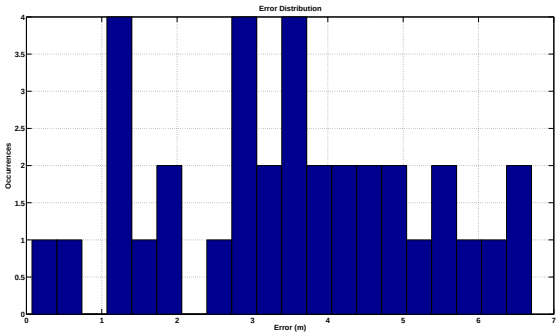

(a)

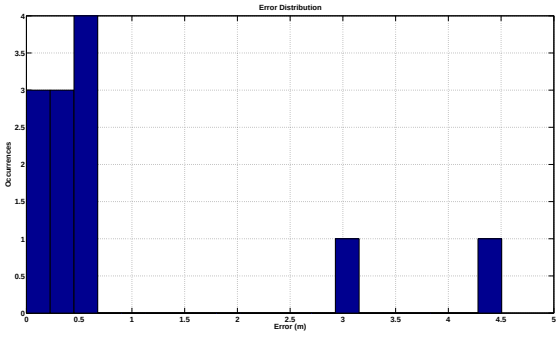

(b)

Fig. 6. Error Distribution Bayesian Method Scenarios 2-3

Table VI shows the performance parameters for both scenarios 2-3 for the Bayesian Method.

Figure 7 shows the distribution of the localization error for the Tomographic method for the **Scenario 2** . Precisely, the picture 7(a) shows the distribution for the only VRTI

TABLE VI
PERFORMANCE PARAMETERS SCENARIOS 2 AND 3 BAYESIAN METHOD

Scenario	RMSE (m)	75-th percentile (m)	90-th percentile (m)
2	3.88	4.7	5.8
3	1.62	0.47	3.55

estimation, while the picture 7(b) shows the distribution for the VRTI estimation filtered out by Kalman.

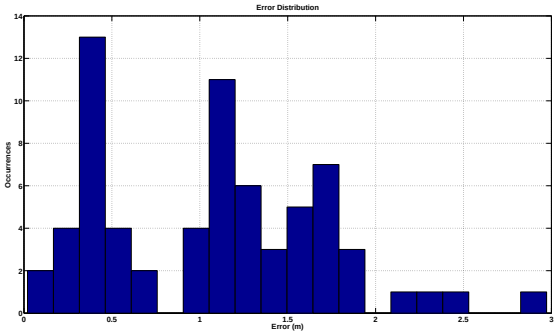

(a)

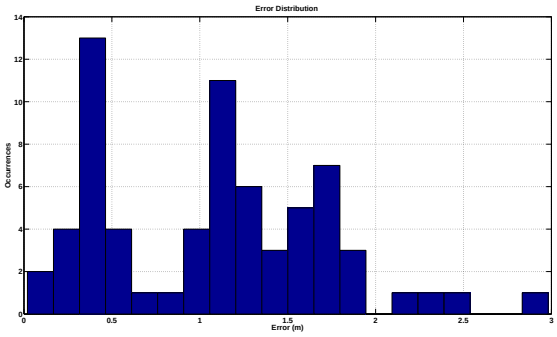

(b)

Fig. 7. Error Distribution Tomographic Method Scenario 2

The figure 8 shows the distribution of the localization error for the Tomographic method for the Un-Noised Model for the **Scenario 2** . Precisely, the picture 8(a) shows the distribution for the only VRTI estimation, instead the picture 8(b) shows the distribution for the VRTI estimation filtered out by the Kalman.

Figure 9 shows the distribution of the localization error for the Tomographic method for the **Scenario 3** . Precisely, the figure 9(a) shows the distribution for the only VRTI estimation, instead the picture 9(b) shows the distribution for the VRTI estimation filtered out by Kalman.

Figure 10 shows the distribution of the localization error for the Tomographic method for the Un-Noised Model for the **Scenario 3** . Precisely, the figure 10(a) shows the distribution for the VRTI estimation only, while the figure 10(b) shows the distribution for the VRTI estimation filtered out by the Kalman.

Table VII and table VIII show the performance parameters for the scenarios 2-3 for the Tomographic Method and for the

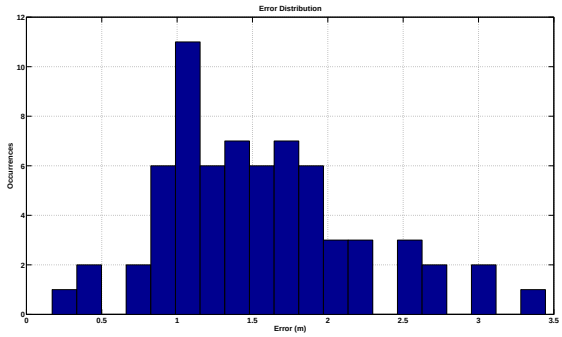

(a)

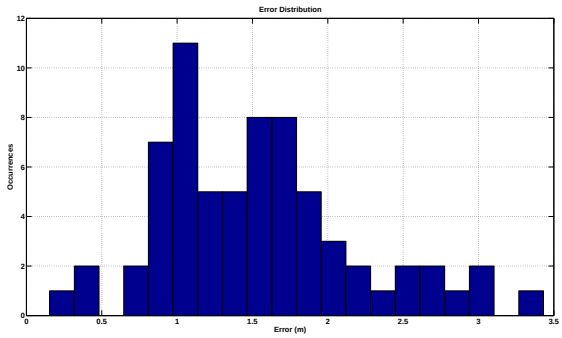

(b)

Fig. 8. Error Distribution Tomographic Method Scenario 2 Un-Noised Model

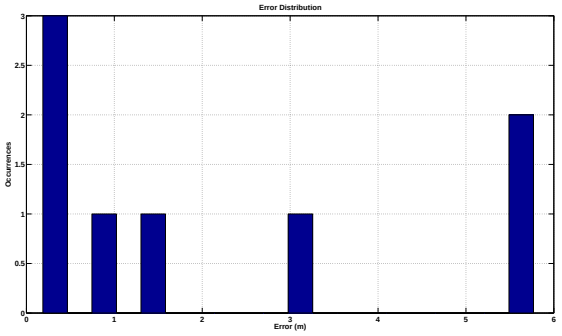

(a)

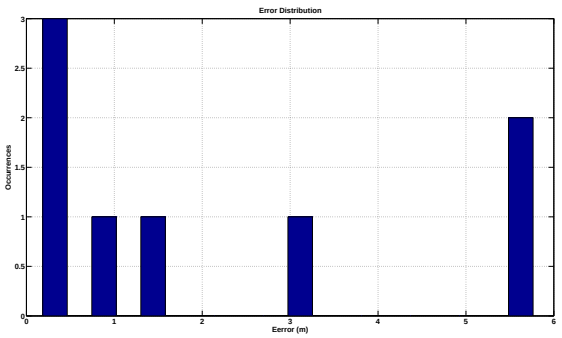

(b)

Fig. 9. Error Distribution Tomographic Method Scenario 3

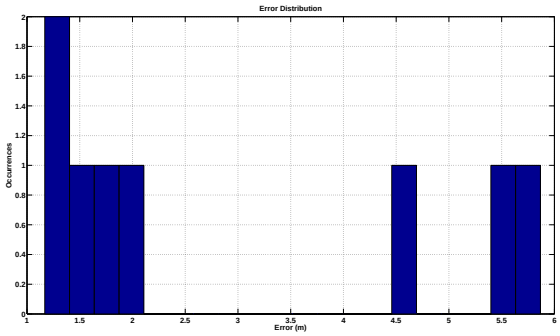

(a)

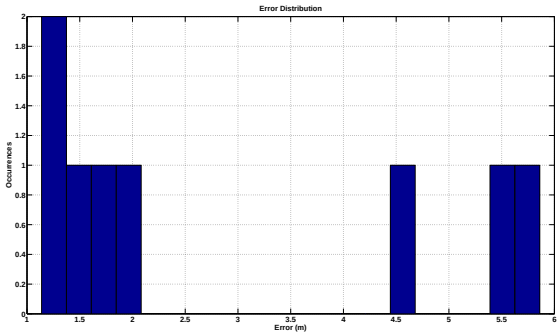

(b)

Fig. 10. Error Distribution Tomographic Method Scenario 2 Un-Noised Model

Tomographic Method for the Un-Noised Model, respectively. In both the tables the values in the first and third rows refer to the VRTI estimation instead the values in the second and forth rows refer to the VRTI values filtered out by Kalman.

TABLE VII
PERFORMANCE PARAMETERS SCENARIOS 2-3 TOMOGRAPHIC METHOD

RMSE (m)	75-th percentile (m)	90-th percentile (m)
	Scenario 2	
1.26	1.55	2
1.26	1.55	1.97
	Scenario3	
3.06	4.24	5.60
3.05	4.23	5.59

TABLE VIII
PERFORMANCE PARAMETERS SCENARIOS 2-3 TOMOGRAPHIC METHOD UN-NOISED MODEL

RMSE (m)	75-th percentile (m)	90-th percentile (m)
	Scenario 2	
1.66	1.84	2.53
1.67	1.82	2.53
	Scenario 3	
3.52	5.09	5.78
3.51	5.07	5.78

Finally, we provide the performance analysis of the Tomographic Method for the **Scenario 4**. In this case the Bayesian Method is not taken into account because the multi-channel measure of the RSS values is per formed, and the authors of the Bayesian method do not give indication on how to use the multi-channel measures.

Also in this scenario, the Tomographic method has been applied using the algorithm's parameters shown in the table III. Again, the method has been tested assuming as solution for the VRTI the equation (17) first, and that in the equation 18 later. In both cases the Kalman's filters has been applied.

Figure 11 shows the distribution of the localization error using the Tomographic method based on the VRTI estimation.

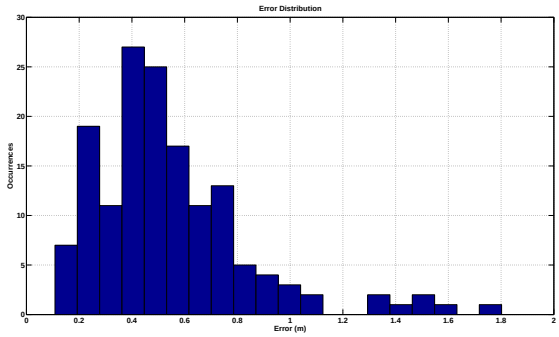

(a)

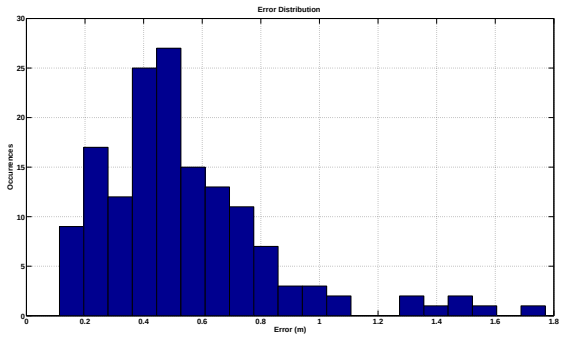

(b)

Fig. 11. Error Distribution Tomographic Method Scenario 4

Figure 11(a) shows the error distribution when only the VRTI is used, instead the figure 11(b) shows the error distribution when the estimated position is also filtered out by Kalman. The figures show that the Kalman filter does not improve the method's performance. In fact the dispersion of the error values is the same as well as the interval of errors with the maximum number of occurrences. These results are confirmed by the performance parameters shown in table IX.

TABLE IX
PERFORMANCE PARAMETERS SCENARIO 4 TOMOGRAPHIC METHOD

RMSE (m)	75-th percentile (m)	90-th percentile (m)
0.62	0.68	1.04
0.62	0.68	1.02

The values in the first row of the table IX refer to VRTI estimation only, while the values in the second row refer to the VRTI values filtered out by the Kalman's filter.

The figure 12 shows the distribution of the localization error using the Tomographic method, assuming equation (17) as a solution of the VRTI , which we call Un-Noised model.

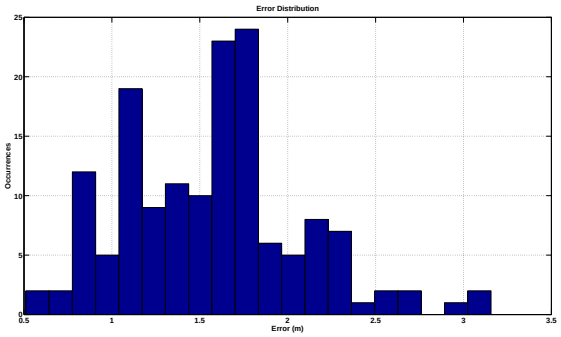

(a)

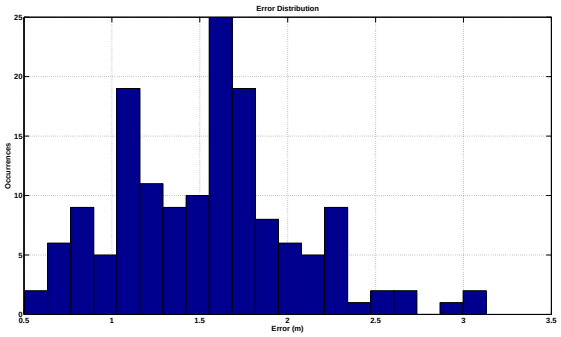

(b)

Fig. 12. Error Distribution Tomographic Method Un-Noised Scenario 1

Figure 12(a) shows the error distribution when the VRTI only is used, while the figure 12(b) shows the error distribution when the estimated position is also filtered out by Kalman. In this case too, the Kalman's filter does not give advantage as shown in the table X .

TABLE X
PERFORMANCE PARAMETERS SCENARIO 1 TOMOGRAPHIC METHOD UN-NOISED MODEL

RMSE (m)	75-th percentile (m)	90-th percentile (m)
1.67	1.85	2.53
1.66	1.83	2.53

Also in this case the error reduction is notable when 17 is used as a solution for the VRTI rather than the solution in the equation 18. In this case, the localization error can be decreased of 63%, moreover, the error dispersion is lower with the first solution than the second one, as the figures 11 and 12 show.

In general, the numerical results show that Bayesian and Tomographic Method for single-channel measure of the RSS have confrontable performance. The multi-channel measures improve the performance of the Tomographic approach, in terms of RMSE, $75-th$ and $90-th$ percentiles . The Kalman filter does not give notable advantage on the estimation. The regularized solution based on the parameters of the measure's error gives better results in the position estimation.

V. CONCLUSION

In this paper we have presented the survey on the localization and tracking algorithms for passive indoor applications, based on WSNs working with the 802.11 or 802.15.4 network protocols. We have introduced the problem of the localization, and in particular the problem addressed in this paper, in the section II, and later in the section III we have provided a comprehensive analysis of the theory behind the algorithms taken into account. Finally, some numerical results have been shown to provide a comparison between the two classes of methods discussed, prediction and Radio Tomography respectively.

Through the prediction methods the RMSE is about $0.77\ (m)$ this result is obtained with about 1 sensor per squared meter of localization area, by the accurate description of target's movements as well as of the measure error. These last two variable are characterized through the a-priori density probability of the target's movement, the error density distribution and the mathematical model for the multi-path phenomenon. These methods make use of the lattice for the definition of the a-priori information and for the calibration phase performed during the algorithm. Obviously the width of the lattice's cells affects the precision of the localization algorithm and its computational performance. In fact, if the cells are too small the localization precision can be high but the computational cost grows exponentially, so that the algorithm is not able to calculate the target position in real time. Moreover, the calibration time of these algorithms is linked to the number of cells. In fact, the calibration values are evaluated cell per cell, in some cases with the target that moves through the cells in other cases without the target. This operation can require many time. Note that, if the topology of the localization area changes the calibration phase should be performed again given that the multi-path effect can drastically change, again if the topology of the area changes also the a-priori information needs to be redefined, given that the cells crossed by the target can change for example.

Through the Radio Tomographic method the RMSE is about $0.62\ (m)$ this result is obtained with about 0.6 sensors per squared meter of localization area, in this case the method not requires any kind of a-priori information to work. The only information required is about the model of the measure error, this information is required by the regularization solution of the VRTI when the measure error is taken into account. The lattice is useful also in this case to evaluate the algorithm's performance, but the width of the cells does not affect the precision of the localization algorithm as in the case of the prediction algorithms. Also in this case the number of cells of the lattice affects the computational cost, given that if the number of cells grows also the dimension of the VRTI grows, and the regularization algorithm can suffer of this growth of dimensionality. In this case the calibration phase is not necessary, intact in our tests this operation has not been performed, obtaining confront able performance with the prediction methods. In this method a changing in the topology of the localization area does not affect the performance

algorithm, given that no information such as the probability to cross a given cell given that the target was in the another one, is required. Finally note that the application of the Kalman's filter does provide performance increasing of 1%, instead the regularization method based on the measure error gives a notable advantage, as well as the multi-channel acquisition of the RSS values.

In the table XI are summarized all the final considerations about the study of the algorithms taken into account.

TABLE XI
COMPARISON PREDICTION METHOD VS RADIO TOMOGRAPHY

	Prediction	Radio Tomography
Sensor Density	1	[0.6-1]
Computational Cost	$O(N_{cells}^2)$ $O(N_{trs}^{1.7})$	$O(3N_{px}Bd^2 + 24N_{px}Bd + 3N_{px})$
Resilience	Very Low	High
Calibration	Required	Not required

Hence, the Sensor Density $(sensors/m^2)$ of two approaches are comparable, even if for the Tomographic method with the multi-channel acquisition this values is the smallest between two methods. The computational cost for the prediction methods is a power of the number of cells N_{cell} and of the number of training set N_{trs} for the Grid-Based Bayesian and SVM method respectively. Instead for the Tomographic method the complexity is the polynomial function of the bandwidth of the matrix W and of the cardinality of the number of pixels N_{px} used to characterize the VRTI. Finally, the prediction approaches require the calibration phase, which can require many time, this phase is not required in the Tomographic method.

REFERENCES

[1] G. Mao, B. Fidan, and B. D.O. Anderson, "Wireless Sensor Network Localization Techniques," *Elsevier Computer Networks*, vol. 51, no. 10, pp. 2529–2553, July 2007.

[2] A. Haeberlen, A. Rudys, E. Flannery, D. S. Wallach, A. M. Ladd, and L. E. Kavraki, "Practical robust localization over large-scale 802.11 wireless networks," in *Proc. ACM Intl. Conf. MOBICOM*, Philadelphia, Pennsylvania, USA, September 2004, pp. 70–84.

[3] C. Xu, Y. Zhao, and Y. Zhang, "Localization technology in wireless sensor networks based on uwb," in *Proc. IEEE Intl. Conf. WNIS*, Shanghai, China, December 2009, pp. 35–37.

[4] A. Falhi, "Localization estimation in wireless sensor networks based on ieee 802.15.4 standard," in *Proc. IEEE Intl. Conf. ICMCS*, Ouarzazate, Morocco, April 2011, pp. 1–6.

[5] C. Morelli, M. Nicolini, V. Rampa, and U. Spagnolini, "Hidden Markov Models for Radio Localization in Mixed LOS/NLOS Conditions," *IEEE Transaction on Signal Processing*, vol. 5, no. 4, pp. 1525–1542, April 2007.

[6] and Crossbow and Technology, "IRIS Datasheet," http://bullseye.xbow.com:81/Products/productdetails.aspx?sid=264, 2013.

[7] S. Savazzi, M. Nicoli, and M. Riva, "Radio imaging by cooperative wireless network: Localization algorithms and experiments," in *Proc. IEEE Intl. Conf. WCNC*, Paris, France, April 2012, pp. 1–5.

[8] A. E. Kosba, A. Saeed, and M. Youssef, "Rasid: A robust wlan device-free passive motion detection system," in *Proc. IEEE Intl. Conf. PCC*, Lugano, Switzerland, March 2012, pp. 180–189.

[9] F. Viani, M. Martinelli, L. Ioriatti, M. Benedetti, and A. Massa, "Passive real-time localization through wireless sensor networks," in *Proc. IEEE Intl. Conf. IGARSS*, Cape Town, South Africa, July 2009, pp. 718–721.

[10] J. Wilson and N. Patwari, "Radio Tomographic Imaging with Wireless Networks," *IEEE Transaction on Mobile Computing*, vol. 9, no. 5, pp. 621–632, May 2010.

[11] M. S. Arulampalam, S. Maskell, N. Gordon, and T. Clapp, "A Tutorial on Particle Filters for Online Nonlinear/Non-Gaussian Bayesian Tracking," *IEEE Transaction on Signal Processing*, vol. 50, no. 2, pp. 174–188, February 2002.

[12] J. M. Aughenbaugh and B. R. La Cour, "Measurement-Guided Likelihood Sampling for Grid-Based Bayesian Tracking," *JOURNAL OF ADVANCES IN INFORMATION FUSION*, vol. 5, no. 2, pp. 102–127, December 2010.

[13] R. Srinivasan, *Importance Sampling*. SPRINGER, 2002.

[14] W. H. Press, S. A. Teukolsky, W. T. Vetterling, and B. P. Flannery, *Numerical Recipes*. Cambridge University Press, 2007.

[15] V. Vapnik, *Statistical Learning Theory*. New York: Wiley, 1998.

[16] A. Massa, A. Boni and M. Donelli, "A Classification Approach Based on SVM for Electromagnetic Subsurface Sensing," *IEEE Tran. On Geoscience and Remote Sensing*, vol. 43, no. 9, pp. 2084–2093, September 2005.

[17] J. Platt, *Probabilistic outputs for support vector machines and comparison to regularized likelihood methods*. Cambridge, MA: Advances in large margin Classifiers, MIT Press, 1999.

[18] A. W. Bowman, "A comparative study of some kernel-based nonparametric density estimators," *J. Statist. Comput. Simul.*, vol. 21, no. 1, pp. 313–327, April 1985.

[19] J. Wilson, N. Patwari, and F. G. Vasquez, "Regularization methods for radio tomographic imaging," in *Proc. Virginia Tech Wireless Symposium*, Virginia, USA, June 2009, pp. 1–9.

[20] H. W. Engl, M. Hanke, and A. Neubauer, *Regularization of Inverse Problems*. SPRINGER, 2004.

[21] K. Ossi, M. Bocca, and N. Patwari, "Enhancing the accuracy of radio tomographic imaging using channel diversity," in *IEEE Int. Conf. MASS*, Las Vegas, Nv, October 2012, pp. 1–9.